Development of a Stress Monitoring System Architecture for Heart Rate Measurement

Gulnur Tyulepberdinova
Al-Farabi Kazakh National University, Almaty, Kazakhstan
tyulepberdinova@gmail.com

Murat Kunelbayev
Al-Farabi Kazakh National University, Almaty, Kazakhstan | Institute of Information and Computing Technologies, Almaty, Kazakhstan
murat7508@yandex.kz

Gulshat Amirkhanova
Al-Farabi Kazakh National University, Almaty, Kazakhstan
gulshat.aa@gmail.com

Miras Tokhtassyn
Al-Farabi Kazakh National University, Almaty, Kazakhstan
mirastoktasyn30@gmail.com (corresponding author)

Alikhan Amirkhanov
Al-Farabi Kazakh National University, Almaty, Kazakhstan
alikhan.amirkhan@gmail.com

Received: 8 July 2025 | Revised: 19 August 2025, 5 September 2025, and 18 September 2025 | Accepted: 19 September 2025

 DOI: https://doi.org/10.48084/etasr.13150

ABSTRACT

This paper presents the development and experimental validation of a wearable system for stress and cardiovascular monitoring that integrates three sensors: a Photo-Plethysmography (PPG) sensor, a Galvanic Skin Response (GSR) sensor, and a DS18B20 digital temperature sensor. The ESP32 microcontroller serves as the core of the system, performing signal filtering using the Exponential Moving Average (EMA) method and lightweight on-device classification with machine learning models (CNN, LSTM). Wireless communication is enabled using Wi-Fi and Bluetooth Low-Energy (BLE), allowing remote monitoring and cloud-based analytics. The system was tested on 10 volunteers under various physical and emotional scenarios, including sitting, walking, exercising, yoga, cycling, and watching movies. The results demonstrated significant physiological variations: the heart rate increased from 75 bpm at rest to 125 bpm during stress episodes, the skin conductance increased by up to 25%, and body temperature changed by 2-3°C depending on activity level. The embedded ML models achieved a stress classification accuracy of 92% (F1 = 0.90). The prototype also showed high energy efficiency, operating for more than 12 hours on a single charge. The proposed architecture offers promising applications for personalized health monitoring, stress management, and integration with medical information systems (FHIR, HL7).

Keywords-stress monitoring; cardiovascular indicators; wearable devices; machine learning; IoT; wireless data transmission

I. INTRODUCTION

Stress is an integral part of human life that significantly affects well-being and quality of life. The need to understand and manage stress has become particularly urgent in recent years, as global events such as the COVID-19 pandemic, political instability, and economic perturbations have dramatically increased the prevalence of stress-related mood and anxiety disorders around the world [1]. This psychological state is not merely an abstract feeling, but is accompanied by distinct physiological responses. Extensive research has established a correspondence between subjective emotional

experience of stress and measurable changes in the body, particularly within the cardiovascular and autonomic nervous systems [2]. Therefore, the development of accessible and reliable technologies for monitoring these physiological indicators is a crucial step toward better stress management and the prevention of its negative health consequences. For instance, data from the Organization for Economic Co-operation and Development (OECD) highlight significant cross-national differences in well-being indicators related to stress. In [3], it was shown that populations in countries such as South Korea, Chile, and the United States reported high levels of stress.

The impact of stress can range from daily annoyances to life-threatening situations. This psychological state is not simply an abstract feeling, but is accompanied by distinct physiological responses. Stress manifests itself through a combination of well-documented emotional and physical symptoms, which correspond to measurable changes in the body [4]. Effective stress management plays a key role in maintaining a normal heart rhythm. It is well-established that monitoring cardiovascular indicators is crucial for tracking changes that can negatively affect health. For example, resting heart rate is a critical vital sign, and changes in its baseline can predict adverse health outcomes and reflect the state of physiological homeostasis [5]. Modern wearable technologies enable this monitoring by analyzing Pulse Rate Variability (PRV), which is obtained from optical sensors such as Photo-Plethysmography (PPG). This metric provides deep insight into the activity of the autonomic nervous system, which is directly affected by stress [6]. To solve this problem, it is necessary to develop accessible, cost-effective, and quality devices that can simplify heart rate monitoring.

The rapid advancement of wearable sensor technology has paved the way for new approaches to continuous health monitoring. In particular, recent progress in flexible and biocompatible sensors has significantly improved the ability to track key physiological indicators in real-time [7]. Such devices have been shown to have an affordable cost and ease of use. Wearable sensors can be integrated with Internet of Things (IoT) technologies, expanding their functionality. The use of Galvanic Skin Response (GSR) for the detection of stress states has been previously examined [8]. The MAX30102 sensor has been applied to the diagnosis of viral diseases, with particular attention to the measurement of oxygen saturation (SpO_2) and Heart Rate (HR) [9]. The integration of biomedical sensors with smartphones facilitates remote health monitoring and improves medical supervision efficiency [10].

The use of PPG for stress assessment is a common approach in modern wearable systems. To improve accuracy, recent studies have focused on the development of multimodal devices. For instance, some studies presented wearables that integrate both PPG and GSR signals for more robust real-time stress detection [11]. Other approaches have successfully applied deep learning models, such as Convolutional Neural Networks (CNNs), to analyze PPG data and automatically recognize stress patterns [12]. This study showed that combining different types of sensors improves measurement accuracy and expands the data collection capabilities. In [13], PPG sensors were used to determine stress levels, with the results confirming that wearable devices can reliably assess stress by analyzing the Autonomic Nervous System (ANS) balance. Recent studies demonstrate the feasibility of MAX30100-based health monitoring systems with wireless connectivity. For example, in [14], an IoT solution used ESP32 and Bluetooth, while in [15], a portable PPG monitor with real-time data transmission through ESP32 was developed. Previous works used this sensor to measure HR and SpO_2 to assess stress levels. In [16], a method was proposed to combine HR data obtained from PPG sensors with video devices. In [17], it was emphasized that changes in HR can serve as stress indicators, and an irregular heartbeat can indicate the presence of serious diseases or other health problems.

The study in [18] investigated the determination of stress levels using commercially available smartwatches. Such devices use Electrodermal Activity (EDA) sensors to detect stress states. However, the results showed that the EDA indicators may not be sufficiently accurate when using only one wearable device. In [19], a wearable belt was used to assess stress levels, establishing that budget sensors can effectively handle this task, despite a significant drawback—large device dimensions. In [20], smartwatches were used to determine mental stress in real-time during various cognitive tasks. This study relied on GSR, RR interval, and Body Temperature (BT) data collected using commercial wearable devices. This study noted that factors such as listening to music during exercise can affect HR, which can lead to a misinterpretation of stress levels [21]. Heart Rate Variability (HRV) at rest is a well-established indicator of stress and overall health [5]. Short-term stressors, including physical activity, can significantly alter HR patterns, as demonstrated in wearable sensor studies [22, 23]. In addition, wearable sensors can be integrated with the IoT to expand their functionality. Recent advances in IoT-fog-cloud computing models have shown promising results in addressing latency issues and improving real-time processing capabilities for health monitoring applications. The integration of fog computing with IoT devices enables edge processing, reducing data transmission delays and energy consumption while maintaining high accuracy in the prediction of cardiovascular diseases [24].

The purpose of this study was to analyze the influence of various types of activities, including watching horror movies, sitting, walking, running, exercising, yoga, and cycling, on human physiological indicators. This study aimed to examine changes in HR, GSR, and body temperature depending on the level of physical activity and emotional state. This study also examined the possibilities of using wearable devices, such as the MAX30102 sensor, for real-time monitoring of the psychophysiological state. Integration of collected data with machine learning algorithms and IoT technologies will allow the development of a personalized health monitoring and stress management system, which can be useful in medical diagnostics, fitness, and the entertainment industry.

Despite growing interest in wearable stress monitoring systems, most existing solutions are limited to a single type of sensor and lack comprehensive validation in real-life conditions. Recent publications rarely feature the integration of

multiple physiological signals—such as PPG, GSR, and skin temperature—in combination with the implementation of machine learning algorithms directly on resource-constrained wearable devices for real-time stress detection. Furthermore, the reliability of stress classification and the impact of wireless data transmission technologies in mobile everyday environments remain insufficiently explored. This study aimed to address these gaps by developing a multi-sensor system with embedded machine learning, on-device data processing, and validation across diverse activity scenarios. The main scientific and practical contributions of this work are as follows:

- Develops a multi-sensor wearable device architecture that integrates PPG, GSR, and a temperature sensor for comprehensive monitoring of physiological indicators.
- Performs embedded signal processing using the Exponential Moving Average (EMA) algorithm and lightweight machine learning models (CNN, LSTM) directly on the ESP32 microcontroller.
- Offers integration with IoT technologies (Wi-Fi, BLE) for wireless data transmission and cloud analytics, including compatibility with medical information systems such as FHIR and HL7.
- Experimental validation in real-life activity scenarios (sitting, walking, exercising, yoga, watching movies) confirms the reliability of measurements and the system's ability to capture stress responses.
- Demonstrates energy efficiency and device autonomy, enabling long-term use in medical and domestic applications.

II. METHOD

The proposed method consists of real-time monitoring of physiological parameters using a wearable device that integrates PPG (MAX30102), GSR, and temperature (DS18B20) sensors. Raw sensor data are filtered using EMA, and relevant features—such as HR, skin conductivity, and temperature changes—are extracted using the ESP32 microcontroller. Lightweight machine learning models, trained on annotated physiological datasets, are deployed on the device to classify stress states in real time. The results and raw data are wirelessly transmitted to a smartphone or cloud platform via BLE and Wi-Fi for further analysis and user feedback.

A. System Architecture

The wearable stress monitoring device developed in this study integrates three main types of sensors: a PPG sensor (MAX30102) for heart rate and SpO_2 measurements, a GSR sensor for electrodermal activity, and a digital temperature sensor (DS18B20) for skin temperature monitoring. The sensors are managed by an ESP32 microcontroller, which also handles wireless communication and local data processing. Figure 1 illustrates the overall system block diagram, detailing the connection of each sensor and key functional modules.

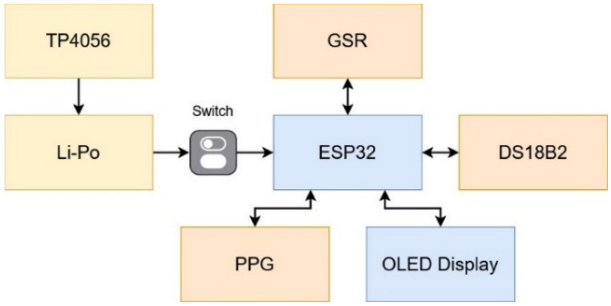

Fig. 1. Block diagram of the wearable stress monitoring device.

The novelty of this work lies in the design and implementation of an innovative stress and cardiovascular monitoring system that integrates several biometric sensors (GSR, PPG, and temperature sensor) to comprehensively analyze physiological parameters in real time. The use of EMA algorithms and machine learning techniques to filter data and predict physiological abnormalities is a novel and suitable technique that improves the accuracy and reliability of stress level and HR monitoring. In addition, wireless technology (BLE and Wi-Fi) can integrate with cloud systems for remote monitoring, which makes the system convenient and accessible to users in real-life environments. The system demonstrates high energy efficiency and stable performance, which is an important step in creating personalized and efficient technologies for healthcare.

The scientific significance of this work is the development of methods to integrate wearable biometric sensors to monitor human physiological conditions such as stress and cardiovascular performance. A system capable of real-time monitoring of changes in heart rate, stress level, and body temperature using multiple sensors (GSR, PPG, DS18B20) is important for improving health monitoring technologies. The application of innovative data filtering algorithms (EMA) and machine learning to analyze biometrics can improve the accuracy of diagnosis and early detection of abnormalities in physiological conditions, which can significantly improve the quality of healthcare and personalized treatment. In addition, wireless data transmission through IoT technologies and cloud platforms opens new opportunities for remote monitoring and integration with medical information systems, which is an important step in the development of remote health monitoring systems.

TABLE I. MODEL AND CHARACTERISTICS OF THE SENSORS USED

Sensor model	Specifications				
	Resolution	**Power supply**	**Interface**	**Measuring range**	**Accuracy**
MAX30102	16-19 bits	1.8-3.3V	I2C	N/A	N/A
DS18B20	9-12-bits	3.0-5.5V	1-Wire	-55°C to +125°C	±0.5°C*

a. From -10°C to +85°C. Accuracy is ±2°C over the full range.

The system utilizes modern sensors that provide high measurement accuracy. The main component is the MAX30102 sensor, which has a resolution of 16-19 bits,

transmits data via the I2C interface, and operates on a 1.8-3.3V power supply, making it energy efficient.

To measure body temperature, the system uses the DS18B20 digital sensor. It features a 9–12-bit resolution and operates on a 3.0-5.5V power supply. The sensor is capable of measuring temperatures in a wide range from -55°C to +125°C, offering an accuracy of ±0.5°C within the range of -10°C to +85°C, and an accuracy of ±2°C for its full range. With its 1-wire interface support, this sensor can be easily integrated into the system, providing stable readings. The Grove GSR sensor measures the electrical conductivity of the skin. The sensor operates in analog format, using a range of 0-1023 ADC values to capture the smallest changes associated with the user's emotional state. The collected data is displayed through a 1.3" OLED display with a resolution of 128×64 pixels, connected through an I2C interface, which provides a clear visualization of information, especially important for wearable devices.

The central computing unit of the system is the ESP32, which processes incoming data, analyzes signals using machine learning algorithms, and transmits them via Wi-Fi or BLE to cloud services or a mobile application. This microcontroller is equipped with a dual-core Tensilica LX6 processor (240 MHz) and supports a wide range of interfaces (I2C, SPI, UART, PWM, ADC), making it ideal for IoT solutions.

B. Hardware Implementation

Figure 2 highlights the compact arrangement of the ESP32 microcontroller, sensor modules, OLED display, and rechargeable Li-Ion battery on a custom PCB. The modular design facilitates convenient testing and sensor replacement if required. Figure 3 provides a detailed sensor connection schematic, specifying power, signal, and interface lines between all sensors and the ESP32.

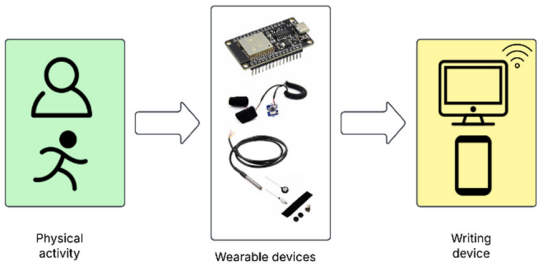

Fig. 2. Photograph of the assembled wearable prototype.

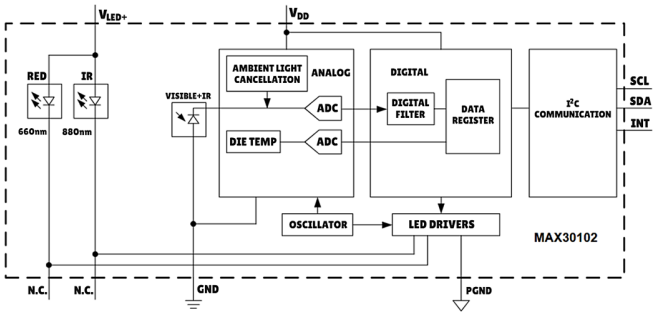

Fig. 3. Schematic diagram of sensor connections to the ESP32 microcontroller.

C. Experimental Setup

Experimental validation was conducted with ten healthy volunteers (age 21–36, balanced by gender) under the supervision of the University's ethics committee. Participants wore the device on the non-dominant wrist, and data were continuously collected during a series of controlled activities: seated rest (baseline), walking, physical exercise (push-ups), yoga, cycling, and emotional stress induced by horror movie viewing. Each scenario lasted 10–20 minutes, with synchronized video annotation and subjective stress rating collected post-session (Likert scale).

The proposed architecture combines high-precision sensors, energy-efficient computing components, and wireless technologies, making it effective for continuous real-time monitoring of physiological parameters. ESP32 via Wi-Fi (TLS) collects and processes data (sensors, accelerometer, machine learning), saves it locally in case of connection loss, transmits it to a smartphone/cloud, notifies the user, monitors the charge, and terminates with the results saved. The novelty of this algorithm lies in the integrated approach to data processing and transmission. The features include the use of machine learning to analyze data directly on the device, which speeds up processing and improves diagnostic accuracy. The system also provides a high level of data security using TLS/SSL encryption during data transmission. An interactive smartphone user interface allows users to view real-time results, receive notifications, and customize monitoring settings, making the process convenient and accessible. In addition, the algorithm can adapt to dropped connections by storing data locally and synchronizing it when the connection is restored, ensuring the integrity and continuity of monitoring.

D. Signal Processing and Data Management

All sensor signals are sampled and preprocessed on the ESP32: Raw data undergoes noise filtering via EMA, artifacts are detected using moving window statistics and thresholding, and key features (HR, GSR peaks, temperature change) are extracted and timestamped. Figure 4 illustrates the data processing workflow.

E. Embedded Machine Learning

For on-device stress detection, lightweight machine learning models are deployed on the ESP32 using TensorFlow Lite Micro. A CNN is used for PPG time-series feature extraction and stress event detection. An LSTM is used for temporal pattern analysis across all sensor channels. Both models were pre-trained on labeled physiological datasets and quantized for embedded inference.

F. Wireless Communication

The device supports dual-mode wireless connectivity:

- BLE (Bluetooth Low Energy) for smartphone app integration and user notifications.
- Wi-Fi (with TLS/SSL) for secure data upload to a cloud server and remote monitoring.

Data can be visualized in real time on both the OLED display and the mobile application.

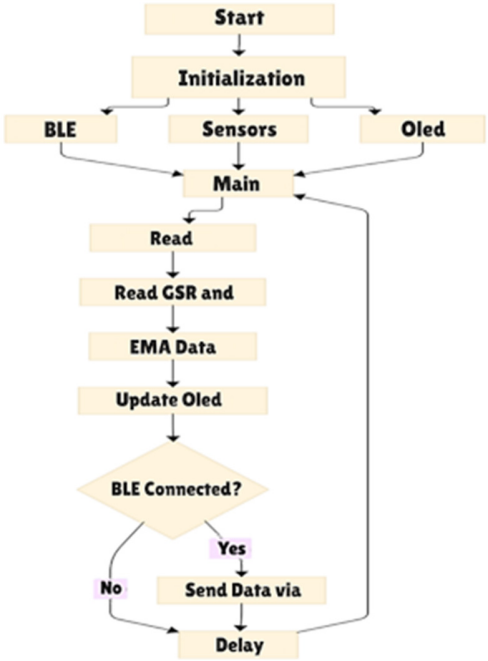

Fig. 4. Workflow of sensor data processing and transmission.

G. Data Analysis

Collected data was statistically analyzed for mean, standard deviation, and range within each scenario. ML model performance was evaluated using standard classification metrics: accuracy, F1-score, and confusion matrix, with scenario-specific stress annotations as ground truth.

III. MATHEMATICAL MODEL AND JUSTIFICATION OF THE METHOD

A. Formalization of Sensor Signals

The system utilizes three types of biosignals represented in the time domain:

$$x_{PPG}(t), x_{GSR}(t), x_T(t) \quad (1)$$

where $x_{PPG}(t)$ is the photoplethysmography signal, $x_{GSR}(t)$ is the GSR signal, and $x_T(t)$ is the digital temperature sensor signal. The signals are discretized with a sampling frequency f_S, and then, their discrete representations are used:

$$x_{PPG}[n] = x_{PPG}(nT_s) \quad (2)$$

$$T_S = \frac{1}{f_S} \quad (3)$$

These signals are time-dependent functions and are influenced both by physical activity (walking, exercising, yoga, cycling) and by psycho-emotional state (stress, arousal, relaxation). For example, during emotional tension, an increase in HR, a rise in skin conductance, and a slight elevation in temperature are observed. In contrast, during relaxation or meditation, the indicators tend to stabilize. By formalizing the sensor signals as time series, it becomes possible to apply further processing methods, such as digital filtering, feature extraction, and machine learning algorithms, for the automatic classification of stress states.

B. Filtering and Preprocessing

The raw signals obtained from the sensors are subject to various sources of noise, such as:

- Motion artifacts (during walking or physical exercise),
- Electromagnetic interference,
- Sensor measurement errors.

The EMA method is applied to suppress noise:

$$y(n) = \alpha x[n] + (1-\alpha)y[n-1], 0 < \alpha < 1 \quad (4)$$

where $x[n]$ is the current sample of the signal, and $y[n]$ is the smoothed value. The EMA filter is stable, since its impulse response given by

$$h[k] = \alpha(1-\alpha)^k, \text{k>0} \quad (5)$$

is absolutely summable:

$$\sum_{k=0}^{\infty}|h[k]| = \frac{\alpha}{1-(1-\alpha)} = 1 < \infty \quad (6)$$

The noise variance after applying the EMA is reduced according to the following formula:

$$\sigma_{out}^2 = \frac{\alpha}{2-\alpha}\sigma_{in}^2 \quad (7)$$

This explains the effectiveness of EMA for PPG and GSR signals. Thus, EMA provides a compromise between smoothing and preserving informative signal variations. For PPG and GSR, this method is particularly effective, as it allows characteristic peaks and trends associated with physiological reactions of the body to be highlighted, while maintaining a minimal level of processing delay.

C. Feature Extraction

After filtering and smoothing, the signals are used to extract physiological parameters that can serve as indicators of stress states and physical workload.

1) Heart Rate (HR)

HR is the primary parameter obtained from the PPG signal. It is determined by counting the peaks of the pulse wave over a fixed time interval T:

$$HR = \frac{N}{T} * 60 \quad (8)$$

where N is the number of detected peaks within the interval T. An increase in HR is usually observed during physical activity or emotional stress, which makes this parameter a key indicator for monitoring the state of the human body.

2) Heart Rate Variability (HRV)

In addition to the average heart rate, HRV is an important diagnostic indicator. It is calculated based on the sequence of RR intervals (the time between successive heartbeats). HRV is determined from the series of RR intervals as follows:

$$HRV = \sqrt{\frac{1}{M}\sum_{i=1}^{1}(RR_i - \overline{RR})^2} \quad (9)$$

A decrease in HRV is often indicative of increased activity of the sympathetic nervous system and is associated with stress.

3) Galvanic Skin Response (GSR)

Electrodermal activity (Galvanic Skin Response - GSR) reflects changes in the electrical conductance of the skin, which are associated with the activation of sweat glands under the influence of stress factors. For normalization, the deviation of the signal from its mean value is used:

$$f_{GSR}(t) = y_{GSR}(t) - \bar{y}_{GSR} \quad (10)$$

4) Skin Temperature (T)

The skin temperature $T(t)$, measured by a digital sensor, is used as an additional indicator of physiological state. During physical activity and stressful situations, small variations may occur, reflecting the body's thermoregulation processes

$$f_T(t) = y_T(t) \quad (11)$$

D. Mathematical Model of Classification

Based on the extracted features, a multidimensional vector is formed, characterizing the current physiological state of the user:

$$f(t) = [HR, HRV, f_{GSR}, f_T, \dots] \quad (12)$$

where the components of the vector correspond to HR, HRV, GSR, and skin temperature, respectively. For automatic state recognition, a machine learning model (e.g.,CNN or LSTM) is used, which implements a nonlinear mapping:

$$y = ML(f(t); \theta),\ y \in \{0,1\} \quad (13)$$

where $y = 1$ corresponds to stress, and θ represents the trained parameters of the network. The minimization of the loss function $L(\theta)$ is carried out using gradient descent algorithms (such as Adam, RMSP, etc.), which allow the model parameters to be optimized so that it can most accurately distinguish between "stress" and "normal" states.

$$L(\theta) = \sum_{i=1}^{N} [y_i \log(\bar{y}_i) + (1 - y_i) \log(1 - \bar{y}_i) \quad (14)$$

Thus, the classifier represents a decision function that, based on the feature vector $f(t)$, assigns the user to one of two states. A high value of $y \approx 1$ indicates a stress condition, while a low value of $y_i \approx 0$ corresponds to its absence.

E. Error Estimation

When calculating HR from pulse intervals, an error may occur due to inaccuracies in detecting R-peaks (or PPG peaks). If the R-interval is measured with a maximum error ε_{max}, then the HR estimate satisfies:

$$\left|\widehat{HR} - HR_{true}\right| \ll \frac{\varepsilon_{max}}{\tau^2} + \frac{1}{T} \quad (15)$$

F. Classification Reliability

Let the classifier $g(f)$ be Lipschitz continuous with constant L_g, and margin $m = | g(f^*) | > 0$. Then, under noise ξ, if $\| \xi \| \leq m/L_g$, the classification label will not change under sub-Gaussian noise with variance σ^2:

$$P_{err} \leq exp(-\frac{m^2}{2\sigma^2 L_g^2}) \quad (16)$$

G. Data Transmission Model

The developed system provides not only local data processing but also transmission through wireless communication channels (Wi-Fi or BLE) for subsequent storage and analysis in cloud services or medical information systems. In this case, the most important characteristics are the latency and reliability of data transmission. The system latency is given by:

$$\Delta t = \frac{L}{f_S} + t_{in} + t_{net} \quad (17)$$

where L/f_s is the window delay, t_{in} is the ML inference time, and t_{net} is the data transmission time.

Thus, minimizing the overall response time is possible through the optimal choice of the window length L, the use of lightweight ML models, and efficient data transmission protocols. Therefore, the developed architecture not only guarantees correct feature extraction and stress state classification at the embedded device level but also ensures secure and practically error-free data transmission to cloud or medical systems, which is particularly important for integration into e-Health infrastructures.

H. Integral System Model

All the stages considered above can be combined into a unified system of equations that describes the complete operating cycle of the wearable stress monitoring system.

$$\begin{cases} y_{PPG}[n] = EMA(x_{PPG}[n]) \\ y_{GSR}[n] = EMA(x_{GSR}[n]) \\ y_T[n] = EMA(x_T[n]) \\ HR = \frac{N}{T} * 60, HRV = Var(RR) \\ f = [HR, HRV, GSR, T) \\ y = ML(f) \\ \Delta t = \frac{L}{f_S} + t_{inf} + t_{net} \end{cases} \quad (18)$$

where EMA is the exponential moving average used for signal filtering, HR and HRV are the cardiac activity indicators, f is the feature vector, $ML(f)$ is the classifier function (CNN/LSTM) returning the user's state, and Δt is the total delay of processing and data transmission. This integral model reflects the complete operating cycle of the system: from acquiring signals from the sensors to classifying the stress state and transmitting the information to the cloud infrastructure. It demonstrates the interconnection between the sensor level, digital signal processing algorithms, machine learning models, and communication protocols, thus providing a comprehensive description of the device architecture.

IV. RESULTS

The prototype was verified by testing the functions of its components, verifying the measurement results, calibration, current, voltage and power consumption analysis, evaluating the processing time, and testing the data visualization process. A comprehensive analysis was performed to ensure that the developed system functions meet the specified design requirements. The developed instrument is a fixed device based on wireless communication.

A. Biosignal Sensor Schematic for Stress Monitoring

Figure 5 shows a schematic diagram of a biosignal sensor for voltage monitoring. The system was assembled by carefully connecting the MAX30102 sensor to the ESP32 pins as per the schematic: power (3.3V), ground (GND), and I2C lines (GPIO 22 and GPIO 21). Then, the ESP32 was programmed to connect to a Wi-Fi network or BLE for data transfer. Code was written in the Arduino IDE to initialize the Wi-Fi, read the values from the MAX30102 sensor over I2C, and process them in the microcontroller.

B. Device Implementation

The MAX30102 sensor plays a key role in measuring HRV, which is an important part of stress monitoring systems. In the initial stage, careful selection of components, such as the ESP32 microcontroller, sensor, and Wi-Fi module, is crucial. This study used the ESP32 development platform to efficiently manage test data. Next, the prototype was assembled, integrating the MAX30102 sensor with the ESP32 microcontroller to ensure proper connectivity and synchronization. The prototype is a critical element for collecting the physiological data needed for stress analysis. Once the prototype was successfully assembled, the MAX30102 sensor could non-invasively measure HR, providing valuable insights into a person's stress levels.

This study conducted tests in five different activity states: sitting, walking, running, exercising, yoga, and cycling. These conditions allow for a comprehensive study of stress patterns under different physical conditions, investigating how stress levels change with different activities. Figure 6 shows the labeled components of an assembled prototype of a wearable device. In addition, the study includes the introduction of wireless portability by integrating Wi-Fi technology into the stress monitoring system. This feature adds novelty and improves the study by allowing individuals to move freely during stress monitoring without physical limitations. With wireless connectivity, the sensor transmits data to the receiving device in real time, providing immediate access to stress information. Wireless portability also simplifies long-term data collection, allowing continuous monitoring over long periods of time, and opens opportunities for remote monitoring and telemedicine.

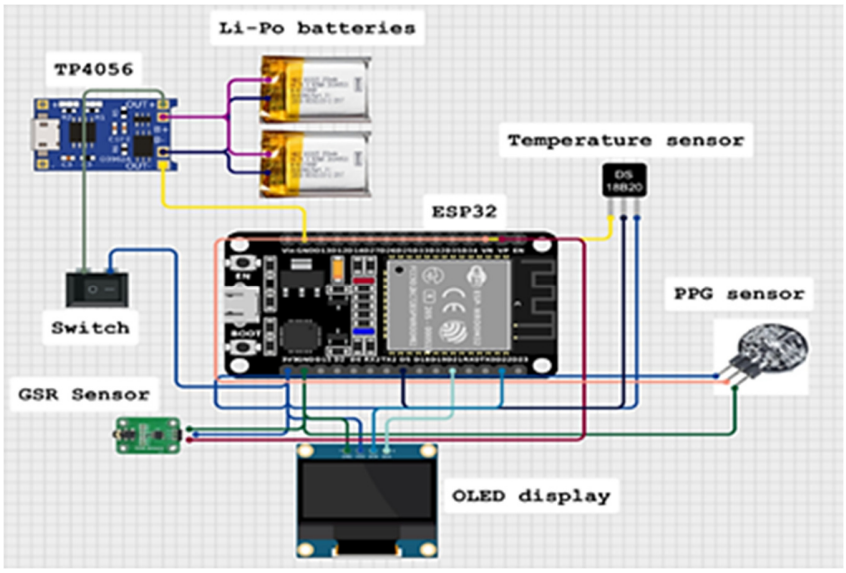

Fig. 5. Schematic diagram of a biosignal sensor for stress monitoring.

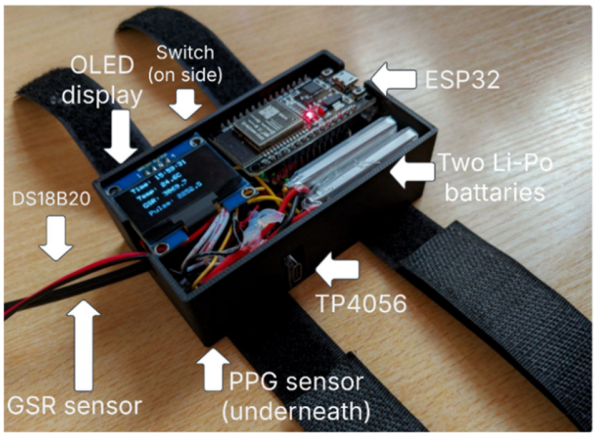

Fig. 6. Labeled components of the assembled wearable device prototype.

Figure 7 shows a measurement of BPM in the seated position using the MAX30102 transducer, which allows for determining resting respiratory rhythm and identifying possible abnormalities. During the test, changes in blood flow reflecting respiratory cycles are recorded, and the average respiratory rate is calculated. Analyzing the data helps identify rhythm stability, abrupt changes, or abnormalities such as rapid (tachypnea) or slow breathing (bradypnea). These indicators are used to assess stress levels, adjust breathing practices, and monitor overall body condition.

Monitoring BPM during walking allows assessing the response of the cardiovascular system to moderate physical activity. The resting HR is first recorded, and then the changes during movement are monitored, including HR adaptation at the beginning, average values during walking, and recovery

rate after stopping. Analyzing the data helps identify rhythm stability, sudden fluctuations, and the level of stress on the body. This approach makes it possible to monitor physical activity, adjust the load, and improve the effectiveness of wellness programs.

Fig. 7. Experimental setup for data collection in a seated, resting position.

Fig. 8. Data collection during moderate physical activity (walking).

Monitoring heart rate (BPM) during exercise makes it possible to assess the level of exertion and the body's adaptation to physical activity. First, initial resting HR readings were recorded, then changes were monitored during the warm-up, the main workout, and the recovery phase. The sensor registers peak and average BPM values, as well as the rate at which the pulse decreases after exertion, which helps determine an athlete's level of fitness. The data obtained make it possible to optimize the training process, prevent overload, and increase the effectiveness of cardio workouts. This approach contributes to a personalized selection of loads and monitoring of the cardiovascular system. Monitoring HR during yoga sessions makes it possible to assess the impact of physical and breathing exercises on the cardiovascular system. First, the pulse is measured at rest, then changes in HR are recorded during static and dynamic asanas, breathing techniques, and relaxation phases. The sensor records peak loads, the average heart rate level, and the recovery rate after exercise. Analyzing the obtained data helps determine the effectiveness of yoga, the influence of various techniques on HR, and develop individual training recommendations. This method allows optimizing exercise loads, controlling stress levels, and assessing the body's adaptation to different types of physical activity.

Fig. 9. Data collection during high-intensity physical activity (push-ups).

Fig. 10. Data collection during a yoga session.

The procedure for measuring HR during cycling involves using a wearable device. Before starting the test, the subject attaches the device to the wrist or another convenient area of the body, ensuring that the sensor fits snugly on the skin. Measurements are taken over a pre-set period, for example, 10–30 minutes, during which HR changes are recorded at various levels of exertion—from a steady pace to intense pedaling. Special attention is given to analyzing the dynamics of HR, detecting abnormalities, and determining load zones, which allows for evaluating endurance and the subject's fitness level. This data can later be used for personalized training recommendations and the prevention of cardiovascular diseases.

Fig. 11. Experimental setup for data collection during cycling.

C. Field Tests

Figure 12 shows the dynamics of skin surface temperature changes during different types of activity. In a seated position (green curve), the temperature remains stable in the range of 27.0–27.3°C, indicating low physical activity and minimal heat generation. During walking (orange curve), the temperature gradually rises, reaching 30.5°C, which is associated with increased muscle activity and accelerated metabolic processes. When performing yoga (dark green curve), the body temperature changes from 28.0°C to 29.7°C, demonstrating a moderate level of physical exertion. In the case of active movement (purple curve), the body temperature increases most significantly, starting from 27.2°C and reaching 31.0°C, reflecting intensive body work and enhanced heat dissipation. This graph shows a pattern where, as physical activity increases, body temperature rises, confirming the relationship between heat generation and activity level.

Figure 13 shows the dynamics of raw signal values from the PPG sensor during different types of activity. These values represent the unprocessed output from the sensor and are proportional to changes in blood volume. In a seated position (green line), the sensor reading remains relatively stable in the range of 1900–2100 units. When performing yoga (dark green line), the signal varies from 2000 to 2500 units. In the case of active movement (purple line), significant fluctuations in the raw signal are observed, ranging from 1900 to 4200 units, including sharp spikes that may indicate high-intensity exertion or additional factors, such as emotional arousal or abrupt changes in activity pace. This graph demonstrates how the body adapts to different types of physical activity and helps identify abnormal HR changes that may signal stress, fatigue, or overload. Figure 14 shows the changes in GSR during different types of activity. During movement (purple line), GSR starts at around 2000 units and gradually increases to about 2300, reflecting high nervous system activity. In a seated position (green line), there is a sharp spike to approximately 2750, after which the level stabilizes. During walking (orange line), GSR values fluctuate in the range of about 2700–2800 but gradually decrease to around 2550, which may be linked to the body's adaptation. During yoga (dark green line), a spike is recorded up to about 3000, followed by a decline to about 2450–2600, reflecting the transition from active arousal to relaxation. This graph illustrates how activity and stress affect skin conductance, with the most significant changes occurring when transitioning from one activity to another.

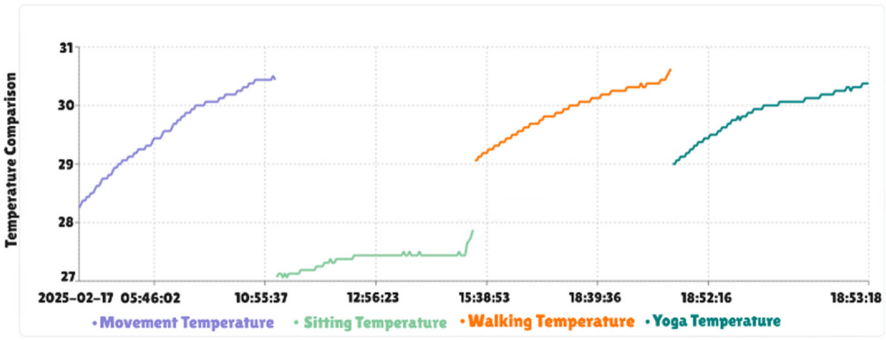

Fig. 12. Temperature(°C) measurements over time.

Fig. 13. Dynamics of raw PPG sensor readings over time. The y-axis represents unprocessed signal amplitude, not beats per minute (BPM).

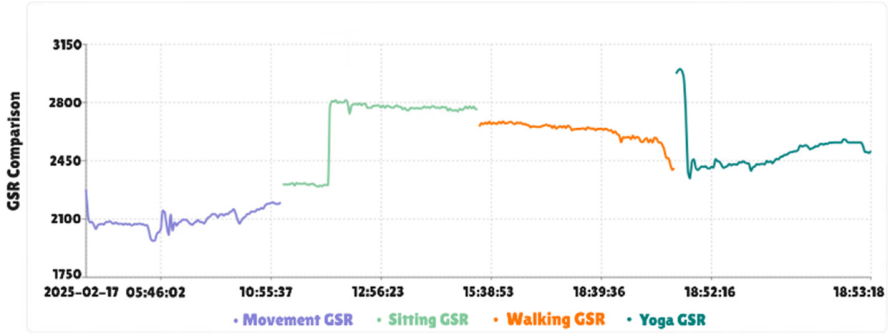

Fig. 14. Electrodermal Activity (EDA) - GSR sensor measurements over time.

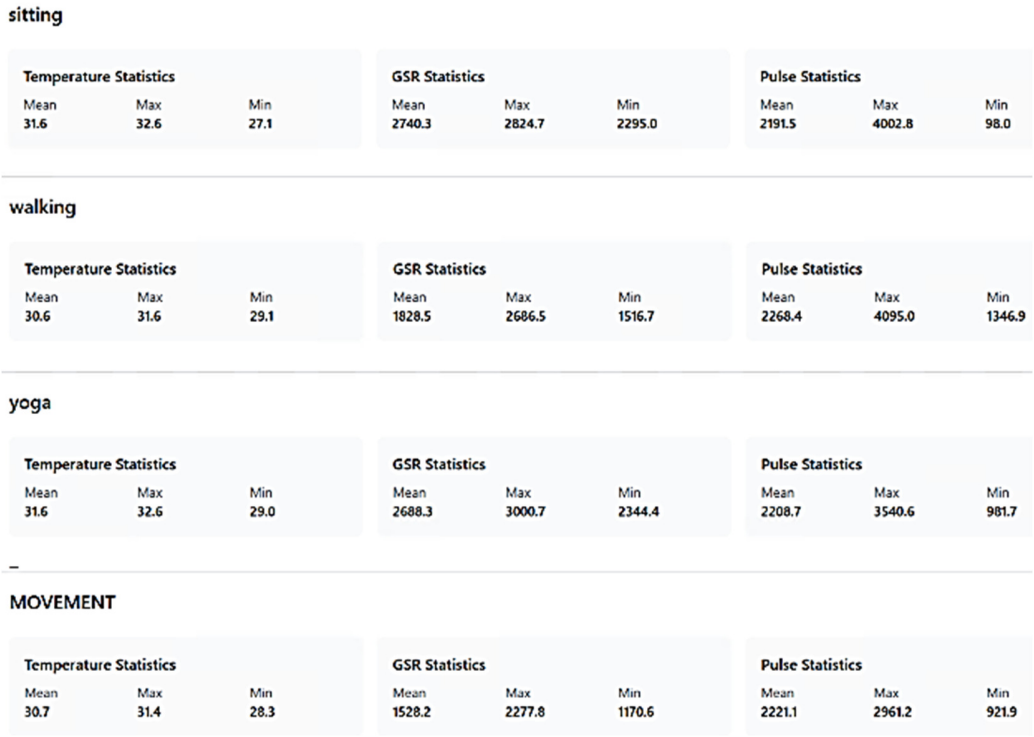

Fig. 15. Simple statistical measurement results.

Figure 15 shows simple statistics for the main statistical indicators of physiological data collected during the experiment:

- Body temperature readings ranged from 27.06°C to 27.13°C, with an average of 27.10°C, indicating the stability of thermoregulation during different activities.
- GSR varied between 2301.58 and 2316.70, with an average of 2308.97, indicating changes in skin conductivity that could be related to physical exertion or emotional state.
- Pulses showed a significant range, reflecting the cardiovascular system's response to different levels of activity.

These data help assess the impact of physical exertion on the body and can be useful for further analysis of changes in physiological parameters over time.

Figure 16 shows the changes in the readings of the PPG sensor over time during physical activity, such as cycling. The x-axis represents the time in seconds, while the y-axis shows the amplitude. In the beginning, there is a smooth increase, which may be linked to the increasing intensity of the exertion. In the middle of the graph, the signal remains at a higher level with slight fluctuations, corresponding to steady physical effort. In the end, there is a gradual decrease, indicating reduced exertion and recovery of the body. These data can be used to analyze endurance, monitor training intensity, and assess the condition of the cardiovascular system.

Figure 17 shows changes in skin surface temperature during a cycling workout. The x-axis represents the time in seconds, while the y-axis shows the temperature in °C. At the beginning of the workout, there is a gradual increase in temperature from 31.5 to 32.2°C, which is associated with increased physical activity and increased heat production in the body. In the

middle of the session, the temperature stabilizes with slight fluctuations, indicating a consistent level of exertion and the body's thermoregulation. At the end of the exercise, the temperature begins to decrease, signaling the recovery process and gradual cooling of the body. These data can be useful for assessing the body's response to physical exertion and identifying any deviations in thermoregulation.

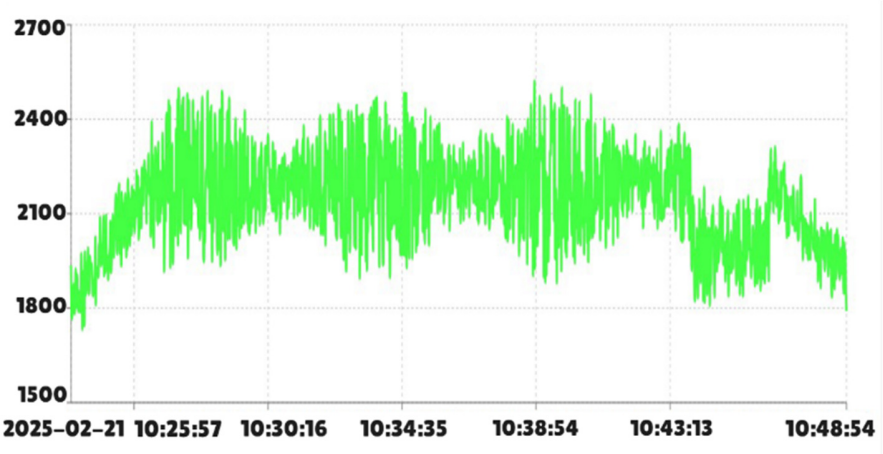

Fig. 16. Changes in raw PPG sensor readings over time during physical activity, such as cycling. The Y-axis shows the unprocessed sensor signal.

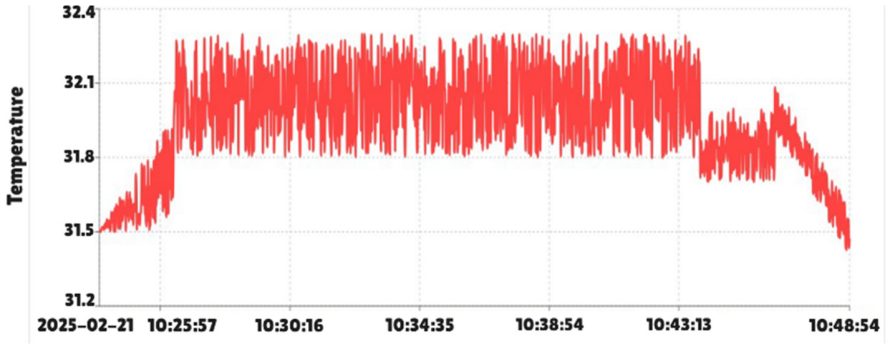

Fig. 17. Changes in body temperature during a cycling workout.

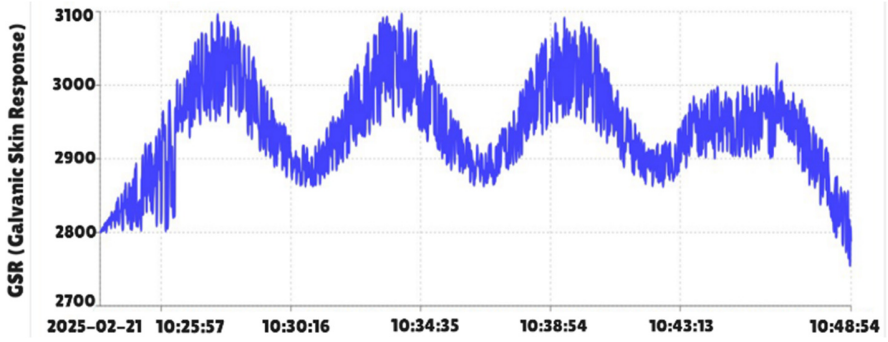

Fig. 18. Changes in GSR during a cycling workout.

Figure 18 shows the changes in GSR during a cycling workout. The x-axis represents time in seconds, while the y-axis shows the GSR values. At the beginning of the workout, there is an increase in GSR from 2800 to 3100, which may indicate initial physical strain and activation of the sympathetic nervous system. Later, GSR values show periodic fluctuations, which may be related to changes in exercise intensity and sweating levels. At the end of the workout, there is a gradual decrease in GSR, indicating a reduction in activity and body recovery. These data can be useful for assessing the level of physical strain and the response of the ANS to exertion.

D. Movie Watching

Wearable devices can be used to analyze the physiological responses of viewers during movie watching. MAX30102 measures HR and SpO_2, helping to identify emotional arousal and stress reactions, along with fluctuations in HRV. Real-time analysis can assess the viewer's level of engagement, reaction

to key moments, and even the potential impact of stress. This data can be useful for psychophysiological research, marketing studies in the entertainment industry, and medical applications related to monitoring the condition of the ANS.

Figure 19 presents the measured temperature results during the viewing of a horror movie, where the subject's body temperature changed noticeably. At the beginning of the session, it was in the range of 28.5°C to 29.5°C, corresponding to a resting state. As the plot developed and tense moments appeared, the temperature gradually increased, reaching a maximum value of 31.35°C, which is associated with the physiological response of the body to stress. During particularly tense moments, brief temperature spikes were observed, triggered by adrenaline release. After the film ended, the temperature began to decrease, returning to 30.4°C, indicating the recovery of normal conditions. These data confirm the influence of emotional tension on the body's physiological parameters.

Figure 20 presents the measured GSR results during the viewing of a horror movie. GSR showed significant fluctuations, indicating the body's physiological response to emotional stimuli. In the beginning, GSR level gradually increased from 2300 to 2700 units, which could be linked to the increasing tension in the plot. During sudden and frightening scenes, spikes in skin conductivity were observed (up to 2900), indicating a brief release of adrenaline. After the peak of activity, roughly in the middle of the movie, the GSR value began to decrease to 2100, likely due to adaptation to stress. However, in the final part, sharp spikes were observed again, which may be related to unexpected scenes or plot twists. At the end of the viewing, the GSR gradually returned to the baseline values, indicating a recovery of emotional state. These data confirm that horror films trigger a strong emotional response, measurable through changes in skin conductivity.

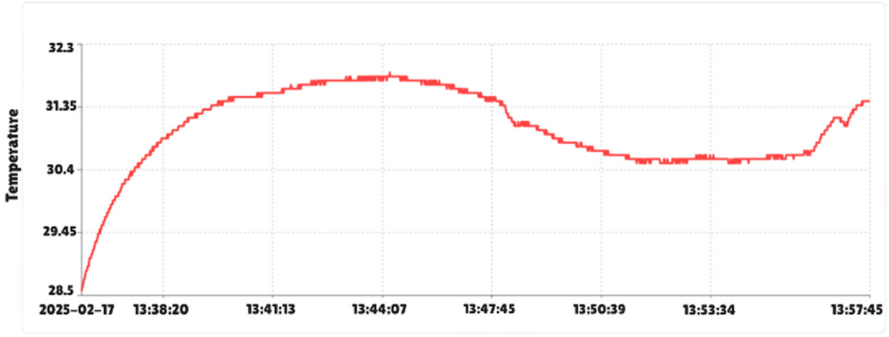

Fig. 19. Measured temperature results during the viewing of a horror film.

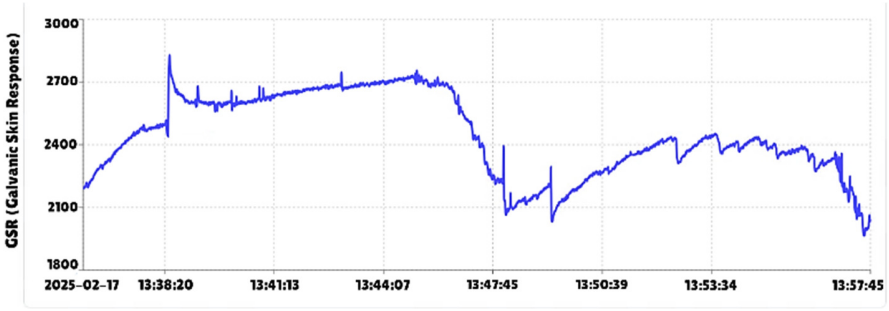

Fig. 20. Measured GSR results during viewing of a horror movie.

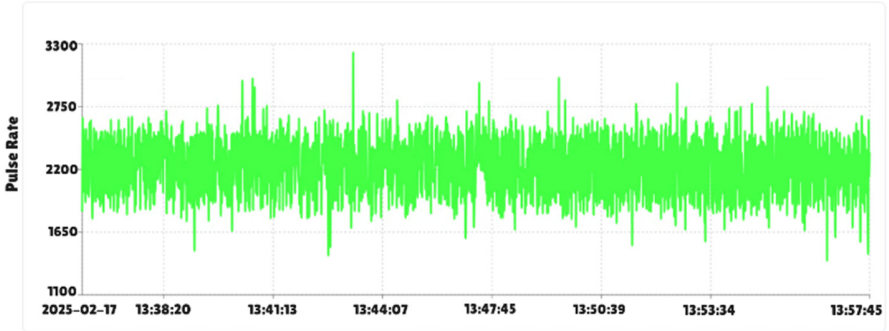

Fig. 21. Measured GSR results during the viewing of a horror movie.

Figure 21 presents the measured raw PPG sensor signal during the viewing of a horror movie. On average, the signal value was in the range of 1650–2200 units, but during tense scenes, there were spikes up to 2750–3300 units. This could be linked to adrenaline release and the body's reaction to sudden, frightening moments. The graph shows that HR remained unstable throughout the viewing, which is typical for situations that induce stress and arousal. The peak values correspond to the scariest scenes, while in the intervals between them, the pulse temporarily decreased but did not reach a level of complete relaxation. These results confirm that horror films trigger a significant physiological response, which can be measured using wearable devices with the MAX30102 sensor.

To provide a physiologically relevant interpretation of the data, the raw PPG signals were processed to calculate HR in beats per minute (bpm). A statistical analysis was performed to assess the reliability of these calculated HR values during the viewing of the horror movie. This included the calculation of the mean (M), standard deviation (SD), and the range of values (Min-Max), as presented in Table II, which shows the final, processed HR data.

TABLE II. MAIN STATISTICAL INDICATORS OF HR

Experiment stage	Average HR (bpm)	Standard deviation	Range (min–max, bpm)
Resting state (before the film)	75.3	5.2	68 – 82
Beginning of the film (waiting)	82.1	6.1	75 – 89
Tense scenes	110.5	9.8	95 – 125
Peak moments (screamers)	125.2	12.3	105 – 140
End of the film	95.8	7.6	85 – 108
Recovery (5 minutes after)	78.5	5.4	70 – 85

Statistical analysis of the changes in HR (bpm) during the viewing of a horror movie showed significant fluctuations depending on emotional tension. In a calm state, the average HR was 75.3 bpm, and during the anticipation of the movie, it rose to 82.1 bpm. During tense scenes, there was a sharp increase to 110.5 bpm, and during peak moments, the maximum values reached 125.2 bpm. After the movie ended, heart rate gradually decreased but remained above the initial level (95.8 bpm), and full recovery took several minutes. The high standard deviation (SD = 12.3 bpm) during peak scenes indicates individual differences in the subjects' reactions. Data analysis confirms that watching horror movies causes significant physiological arousal, and the collected data is reliable and reflects the typical bodily response to stress.

E. Comparison with Other Studies

Many technologies for stress monitoring already exist, but the proposed system provides several key advantages. Unlike solutions that rely on a single sensor (PPG or GSR), the proposed architecture integrates PPG, GSR, and a temperature sensor, improving accuracy and robustness. Furthermore, while most existing approaches perform signal processing and classification externally or in the cloud, the proposed system implements embedded processing on the ESP32 microcontroller using EMA and lightweight machine learning models (CNN, LSTM). This reduces latency and allows the device to operate independently of smartphones or servers. Another important difference is the experimental validation in real-life activity scenarios (walking, yoga, movie watching, etc.), which is rarely addressed in previous studies. Therefore, the proposed system is more practical, energy-efficient, and autonomous compared to existing technologies.

Table III presents a comparison between existing stress monitoring systems [13, 18-20, 23] and the proposed architecture. The analysis shows that most prior works are limited to single-sensor configurations and rely on external or offline data processing, with restricted validation scenarios. In contrast, the proposed system integrates three complementary sensors (PPG, GSR, temperature), implements embedded signal processing and lightweight machine learning models directly on the ESP32 microcontroller, and supports secure wireless connectivity (Wi-Fi, BLE). In addition, the system was validated under diverse real-life activity scenarios, demonstrating higher accuracy, energy efficiency, and practical applicability compared to existing technologies.

TABLE III. COMPARISON OF EXISTING STRESS MONITORING SYSTEMS AND THE PROPOSED SYSTEM

Study/year/(device)	Sensors used	Processing	Connectivity	Validation	Limitations
[13] (2022)	PPG	External, offline	–	Physical effort	Single sensor, not stress-specific
[18] (2019) Smartwatch	GSR, HR	Basic on-device	BLE	Daily activities	Low accuracy, device limitations
[19] (2016)	HR sensor	External analysis	Wired / Bluetooth	Stress tasks	Low-reliability, low-cost sensors
[20] (2017)	GSR + HR (RR)	Basic processing	–	Cognitive stress tasks	Limited multimodality
[23] (2024)	PPG + GSR	AI framework (offline)	–	Laboratory dataset	No embedded system, high complexity
Proposed system	PPG + GSR + Temperature	On-device ML (CNN, LSTM) + EMA filtering	Wi-Fi + BLE (TLS/SSL secure)	Real-life stress scenarios (yoga, cycling, movies)	Compact, energy-efficient, validated in practice

V. CONCLUSION AND FUTURE WORK

This study successfully developed and validated a comprehensive wearable stress and cardiovascular monitoring system that integrates multiple biometric sensors (MAX30102, DS18B20) and an ESP32 microcontroller. The system demonstrated its ability to monitor key physiological parameters in real-time (HR, GSR, and body temperature) across diverse scenarios, including various physical activities and emotional states induced by watching a horror movie. The results unequivocally confirmed the significant impact of both

physical exertion and psychological stress on these physiological indicators, with measurable surges in the raw PPG signal (up to 3300 units), GSR (up to 3000 units), and body temperature (from ~28.5°C to 31.3°C) during high-stress events. The core scientific novelty lies in the synergistic hardware-software architecture: the robust multi-sensor fusion provides comprehensive physiological data, while the application of advanced filtering algorithms (EMA) and machine learning models (CNN, LSTM) directly on the ESP32 microcontroller enables accurate real-time anomaly detection and stress level prediction, significantly enhancing diagnostic reliability beyond single-sensor approaches. Furthermore, the seamless integration of BLE and Wi-Fi facilitates efficient wireless data transmission to cloud platforms and mobile applications, enabling practical remote monitoring and analytics.

The system's design emphasizes high energy efficiency and long-term operational capability on a single charge, making it suitable for deployment in diverse settings, from clinical environments to daily personal health management. This work represents a significant step toward personalized, accessible, and continuous health monitoring, offering valuable tools for stress management, cardiovascular disease prevention, fitness optimization, and potentially psychophysiological research in entertainment contexts. Future research will focus on expanding the capabilities of the system by incorporating additional physiological signals (e.g., ECG), validating the ML models on larger and more diverse populations, refining the algorithms for improved specificity in stress detection across different contexts, exploring integration with medical information systems (e.g., FHIR, HL7), and conducting longitudinal studies to assess the system's efficacy in real-world health management applications, particularly for the target group of students in Kazakhstan.

ACKNOWLEDGMENT

This study was supported by a project from the Ministry of Science and Higher Education of the Republic of Kazakhstan, No. AP23488439 "Development and implementation of IoT-based wearable devices for student stress monitoring in Kazakhstan" (2024-2026).

REFERENCES

[1] H. Akil and E. J. Nestler, "The neurobiology of stress: Vulnerability, resilience, and major depression," *Proceedings of the National Academy of Sciences*, vol. 120, no. 49, Dec. 2023, Art. no. e2312662120, https://doi.org/10.1073/pnas.2312662120.

[2] J. Campbell and U. Ehlert, "Acute psychosocial stress: Does the emotional stress response correspond with physiological responses?," *Psychoneuroendocrinology*, vol. 37, no. 8, pp. 1111–1134, Aug. 2012, https://doi.org/10.1016/j.psyneuen.2011.12.010.

[3] *OECD, How's Life? 2017: Measuring Well-being*. OECD, 2017.

[4] V. J. Clemente-Suárez, P. T. Nikolaidis, B. Knechtle, and P. Ruisoto, "Editorial: Psychophysiology of Stress," *Frontiers in Psychology*, vol. 13, Apr. 2022, Art. no. 896773, https://doi.org/10.3389/fpsyg.2022.896773.

[5] B. Olshansky, F. Ricci, and A. Fedorowski, "Importance of resting heart rate," *Trends in Cardiovascular Medicine*, vol. 33, no. 8, pp. 502–515, Nov. 2023, https://doi.org/10.1016/j.tcm.2022.05.006.

[6] E. Mejía-Mejía, J. M. May, R. Torres, and P. A. Kyriacou, "Pulse rate variability in cardiovascular health: a review on its applications and relationship with heart rate variability," *Physiological Measurement*, vol. 41, no. 7, Aug. 2020, Art. no. 07TR01, https://doi.org/10.1088/1361-6579/ab998c.

[7] S. Chen, J. Qi, S. Fan, Z. Qiao, J. C. Yeo, and C. T. Lim, "Flexible Wearable Sensors for Cardiovascular Health Monitoring," *Advanced Healthcare Materials*, vol. 10, no. 17, Sep. 2021, Art. no. 2100116, https://doi.org/10.1002/adhm.202100116.

[8] X. Yang *et al.*, "The effects of traveling in different transport modes on galvanic skin response (GSR) as a measure of stress: An observational study," *Environment International*, vol. 156, Nov. 2021, Art. no. 106764, https://doi.org/10.1016/j.envint.2021.106764.

[9] B. Annapurna, A. Manda, A. C. Raj, R. Indira, S. P. Kumari, and V. Nagalakshmi, "Max 30100/30102 Sensor Implementation to Viral Infection Detection Based On Spo2 and Heartbeat Pattern," *Annals of the Romanian Society for Cell Biology*, vol. 25, no. 2, pp. 2053–2061, 2021.

[10] S. Majumder, T. Mondal, and M. Deen, "Wearable Sensors for Remote Health Monitoring," *Sensors*, vol. 17, no. 1, Jan. 2017, Art. no. 130, https://doi.org/10.3390/s17010130.

[11] R. R. Sakheran, Q. W. Oung, and H. L. Lee, "A Smartphone-Based Health Monitoring and Management System," in *2024 IEEE 1st International Conference on Communication Engineering and Emerging Technologies (ICoCET)*, Kepala Batas, Malaysia, Sep. 2024, pp. 1–4, https://doi.org/10.1109/ICoCET63343.2024.10730141.

[12] S. Majumder and M. J. Deen, "Smartphone Sensors for Health Monitoring and Diagnosis," *Sensors*, vol. 19, no. 9, May 2019, Art. no. 2164, https://doi.org/10.3390/s19092164.

[13] I. Martínez-González-Moro, I. Albertus Cámara, and M. J. Paredes Ruiz, "Influences of Intense Physical Effort on the Activity of the Autonomous Nervous System and Stress, as Measured with Photoplethysmography," *International Journal of Environmental Research and Public Health*, vol. 19, no. 23, Nov. 2022, Art. no. 16066, https://doi.org/10.3390/ijerph192316066.

[14] K. Singh, P. Thiyagarajan, and P. Sasikumar, "Design and implementation of IoT enabled low cost SPO2 and heart rate monitoring system," in *2022 IEEE Delhi Section Conference (DELCON)*, New Delhi, India, Feb. 2022, pp. 1–6, https://doi.org/10.1109/DELCON54057.2022.9753167.

[15] S. Güder and H. Güder, "Investigation of the Chemical Content and User Comments on Facial Cleansing Products," *Cureus*, vol. 15, no. 5, May 2023, Art. no. e38673, https://doi.org/10.7759/cureus.38673.

[16] X. Liu, W. Wei, H. Kuang, and X. Ma, "Heart Rate Measurement Based on 3D Central Difference Convolution with Attention Mechanism," *Sensors*, vol. 22, no. 2, Jan. 2022, Art. no. 688, https://doi.org/10.3390/s22020688.

[17] C. J. Huang, H. L. Chan, Y. J. Chang, S. M. Chen, and M. J. Hsu, "Validity of the Polar V800 Monitor for Assessing Heart Rate Variability in Elderly Adults under Mental Stress and Dual Task Conditions," *International Journal of Environmental Research and Public Health*, vol. 18, no. 3, Jan. 2021, Art. no. 869, https://doi.org/10.3390/ijerph18030869.

[18] S. Sen, V. Mishra, and D. Kotz, "Using vibrations from a SmartRing as an out-of-band channel for sharing secret keys," in *Adjunct Proceedings of the 2019 ACM International Joint Conference on Pervasive and Ubiquitous Computing and Proceedings of the 2019 ACM International Symposium on Wearable Computers*, London, United Kingdom, Sep. 2019, pp. 198–201, https://doi.org/10.1145/3341162.3343818.

[19] M. Salai, I. Vassányi, and I. Kósa, "Stress Detection Using Low Cost Heart Rate Sensors," *Journal of Healthcare Engineering*, vol. 2016, no. 1, 2016, Art. no. 5136705, https://doi.org/10.1155/2016/5136705.

[20] L. Ciabattoni, F. Ferracuti, S. Longhi, L. Pepa, L. Romeo, and F. Verdini, "Real-time mental stress detection based on smartwatch," Jan. 2017, pp. 110–111, https://doi.org/10.1109/ICCE.2017.7889247.

[21] M. Faulkner *et al.*, "Music Tempo: A Tool for Regulating Walking Cadence and Physical Activity Intensity in Overweight Adults?," *International Journal of Environmental Research and Public Health*, vol. 18, no. 15, Jul. 2021, Art. no. 7855, https://doi.org/10.3390/ijerph18157855.

[22] K. He *et al.*, "Relationship of resting heart rate and blood pressure with all-cause and cardiovascular disease mortality," *Public Health*, vol. 208, pp. 80–88, Jul. 2022, https://doi.org/10.1016/j.puhe.2022.03.020.

[23] S. Barik, V. K. Thakur, M. A. Miah, and S. Pal, "Detection of Stress from PPG and GSR Signals using AI Framework," *Journal of The Institution of Engineers (India): Series B*, Jan. 2025, https://doi.org/10.1007/s40031-024-01191-z.

[24] H. J. Suleiman, I. R. A. Hamid, and O. R. Olaniran, "Smart Health Monitoring for Predicting Heart Disease using IoT-Fog-Cloud Computing Model," *Engineering, Technology & Applied Science Research*, vol. 15, no. 3, pp. 22565–22572, Jun. 2025, https://doi.org/10.48084/etasr.10048.